Available online at www.sciencedirect.com
SCIENCE DIRECT
PHOTONICS AND NANOSTRUCTURES Fundamentals and Applications
Photonics and Nanostructures – Fundamentals and Applications 3 (2005) 100–106
www.elsevier.com/locate/photonics

A time-dependent Green's function approach to study the transient phenomena in metamaterial lens focusing

Lei Zhou [a,b,*], Xueqin Huang [a], C.T. Chan [b]

[a] *Surface Physics Laboratory (State Key Laboratory) and Physics Department, Fudan University, Shanghai 200433, China*
[b] *Physics Department, Hong Kong University of Science and Technology, Clear Water Bay, Kowloon, Hong Kong, China*

Received 15 August 2005; received in revised form 17 September 2005; accepted 18 September 2005
Available online 10 October 2005

Abstract

We applied a time-dependent Green's function approach to study the transient behaviors in metamaterial lens focusing. An adaptive-grid method is developed to deal with the singularities encountered in the numerical integrations and a benchmark result is presented to demonstrate the validity of our theory. We then implement the method to study several typical focusing processes with metamaterial-based lenses.

PACS: 41.20.Jb; 42.30.Va; 78.20.Ci; 42.79.Bh

Keywords: Focusing; Transient behaviors; Super lens; Resolution; Metamaterials; Green's function

1. Introduction

Much recent attention has been paid to a new type of artificial metamaterials, which possesses simultaneously negative ε and μ, and thus a negative refractive index [1]. As one of its potential applications, Veselago proposed to use a flat slab of such metamaterial (with $\varepsilon = \mu = -1$) as a lens to focus electromagnetic (EM) waves [1]. Recently, Pendry showed that such a lens is actually a *perfect* lens, in the sense that not only propagating components, but also all evanescent components radiated from the source could be collected by the lens [2]. The idea of a *perfect* lens was challenged by some researchers, who argued that the field would be divergent if $\varepsilon = \mu = -1$ [3]. Pendry [4] and Smith et al. [5] then showed that the divergence problems could be avoided if ε and/or μ is not *precisely* -1, but has a small deviation δ from -1. The price of adding such a deviation is that the focusing can no longer be perfect. However, the image resolution can still beat the diffraction limit if δ is sufficiently small, so that such a lens is usually called a *super* lens.

Many theoretical works were performed to study this effect [6–14], employing either finite-difference-time-domain (FDTD) simulations [6–11] or some approximate theories [12,14]. Most studies to date considered a two-dimensional (2D) model employing a line source [6–12], and were only interested in the finally stabilized image properties [6–13]. The transient behaviors were neglected in most studies, except for example Ref. [14] in which the relaxation phenomena were examined by a model [14]. While the sources could be strictly *monochromatic*, transient waves are still inevitable, due to the ''switch-on'' process of the source. We note that the transient behaviors might not be important in a conventional lensing problem, but the case for super lens is more subtle. For example, a pioneering FDTD

* Corresponding author. Tel.: +86 2165110575; fax: +86 2165110575.
E-mail address: phzhou@fudan.edu.cn (L. Zhou).

1569-4410/$ – see front matter © 2005 Elsevier B.V. All rights reserved.
doi:10.1016/j.photonics.2005.09.005

simulation showed that no steady foci were found in the *perfect* lens focusing and the fields varied dramatically over time [6]. Later FDTD studies also noticed such oscillations [7], and had to add absorptions to obtain stable images in their simulations [8,9]. Since the employed sources in all FDTD simulations are strictly *monochromatic* [6–11], these unusual phenomena implied that the transient-wave dynamics must be complex and not negligible in such optical processes related to metamaterials.

In reviewing these existing efforts, we feel desirable to develop a rigorous approach that can be used to study quantitatively the transient phenomena in the optical processes related to metamaterials, and, in particular, the metamaterial lens focusing problems. In this paper, we will formulate a time-dependent Green's function approach to serve this purpose. The method has been successfully implemented [15] to explain the image oscillations in the 2D model found previously [6,7] and to predict a new kind of image oscillation behaviors in a three-dimensional (3D) model employing a point source [16]. In this paper, we mainly focus on the details of the theory (Section 2) and the key computational techniques (Section 3). After presenting a benchmark result to test the validity of our theory in Section 3, we present two examples in Section 4 to illustrate the application of this method. We then conclude in the last section.

2. The time-dependent Green's function approach

For the problems we are treating, we assume that a current source of the form $\vec{J}(\vec{r},t)$ is located at the origin, and a slab of metamaterial of thickness d, with a relative permittivity ε_r^L and a relative permeability μ_r^L, is placed at the xy-plane between $z=-d/2$ and $z=-3d/2$ as a lens to focus EM waves radiated from the source. An image will be formed on the plane located at $z=-2d$.

We first consider the simple case where ε_r^L and μ_r^L are both frequency-independent. The problem is then to solve the following Maxwell equations:

$$\nabla\times\vec{E}(\vec{r},t)=-\mu(\vec{r})\frac{\partial}{\partial t}\vec{H}(\vec{r},t),$$
$$\nabla\times\vec{H}=\varepsilon(\vec{r})\frac{\partial}{\partial t}\vec{E}(\vec{r},t)+\vec{J}(\vec{r},t), \tag{1}$$

in an inhomogeneous media described by

$$\varepsilon(r),\mu(r)=\begin{cases}\varepsilon_0,\mu_0 & z>-d/2,\\ \varepsilon_0\varepsilon_r^L,\mu_0\mu_r^L & -d/2>z>-3d/2,\\ \varepsilon_0,\mu_0 & z<-3d/2.\end{cases} \tag{2}$$

We rewrite Eq. (1) as:

$$\nabla\times\nabla\times\vec{E}(\vec{r},t)+\mu(\vec{r})\varepsilon(\vec{r})\frac{\partial^2}{\partial t^2}\vec{E}(\vec{r},t)=-\mu(\vec{r})\frac{\partial}{\partial t}\vec{J}(\vec{r},t). \tag{3}$$

To solve Eq. (3), let us first define a dyadic Green's function $\overrightarrow{\overrightarrow{G}}(r,r';t,t')$ satisfying

$$\left(\nabla\times\nabla\times+\mu(\vec{r})\varepsilon(\vec{r})\frac{\partial^2}{\partial t^2}\right)\overrightarrow{\overrightarrow{G}}(\vec{r},\vec{r}';t,t')=\delta(\vec{r}-\vec{r}')\delta(t-t')\overrightarrow{\overrightarrow{I}}, \tag{4}$$

where $\overrightarrow{\overrightarrow{I}}$ is a unit matrix. If $\overrightarrow{\overrightarrow{G}}(r,r';t,t')$ is known, the E field can be found as

$$\vec{E}(\vec{r},t)=-\mu_0\int\overrightarrow{\overrightarrow{G}}(\vec{r},t;\vec{r}',t')\cdot\vec{J}\cdot(\vec{r}',t')\,\mathrm{d}\vec{r}'\,\mathrm{d}t', \tag{5}$$

where the dot means time derivative. Fourier transforming Eq. (4) from time domain to frequency domain yields:

$$[\nabla\times\nabla\times-\mu(\vec{r})\varepsilon(\vec{r})\omega^2]\overrightarrow{\overrightarrow{G}}(\vec{r},\vec{r}';\omega)=\delta(\vec{r}-\vec{r}')\overrightarrow{\overrightarrow{I}}, \tag{6}$$

where

$$\overrightarrow{\overrightarrow{G}}(\vec{r},\vec{r}';t,t')=\frac{1}{2\pi}\int\mathrm{d}\omega\,\overrightarrow{\overrightarrow{G}}(\vec{r},\vec{r}';\omega)\,\mathrm{e}^{-i\omega(t-t')} \tag{7}$$

is the Green's function in frequency domain. Apparently, when the material is dispersive, we only need to rewrite Eq. (6) as:

$$[\nabla\times\nabla\times-\mu(\vec{r},\omega)\varepsilon(\vec{r},\omega)\omega^2]\overrightarrow{\overrightarrow{G}}(\vec{r},\vec{r}';\omega)=\delta(\vec{r}-\vec{r}')\overrightarrow{\overrightarrow{I}}, \tag{8}$$

where $\varepsilon(\vec{r},\omega)$ and $\mu(\vec{r},\omega)$ are the permittivity and the permeability of the system at this particular frequency. Considering the general properties:

$$\mu(\vec{r},\omega)^*=\mu(\vec{r},-\omega),\quad \varepsilon(\vec{r},\omega)^*=\varepsilon(\vec{r},-\omega), \tag{9}$$

it is easy to prove a very useful relationship:

$$\overrightarrow{\overrightarrow{G}}(\vec{r},\vec{r}';-\omega)=\overrightarrow{\overrightarrow{G}}(\vec{r},\vec{r}';\omega)^*. \tag{10}$$

To proceed, the switch-on process and the space distribution of the current source should be specified. To capture the essence of the physics while keeping the mathematics tractable, we take the simplest "switch-on" process – a step-function in time. For the space distribution, we consider three typical cases in this paper. The first one is a point current source (e.g., the 3D configuration):

$$\vec{J}(\vec{r},t) = \hat{y}P_0\delta(\vec{r})\,\mathrm{e}^{-i\omega_0 t}\theta(t), \tag{11}$$

where ω_0 is the working frequency and P_0 is the strength of the dipole source. A straightforward calculation shows:

$$\dot{\vec{J}}(\vec{r}',t') = P_0\hat{y}\delta(\vec{r}')\,\mathrm{e}^{-i\omega_0 t'}[\delta(t') - i\omega_0\theta(t')]. \tag{12}$$

Inserting Eqs. (7) and (12) into (5), we obtain:

$$\vec{E}(\vec{r},t) = \frac{1}{2\pi}\int \mathrm{d}\omega\,\mathrm{e}^{-i\omega t}\vec{E}^{\,3D}(\vec{r},\omega)\frac{\omega}{\omega-\omega_0+i\eta}, \tag{13}$$

where

$$\vec{E}^{\,3D}(\vec{r},\omega) = -\mu_0 P_0\,\vec{\vec{G}}(\vec{r},0;\omega)\cdot\hat{y}. \tag{14}$$

The positive sign of the infinitesimal number η in Eq. (13) is determined by the requirement that the current source amplitude should be bounded as $t\to\infty$. Later, we will show this choice is also consistent with causality.

Let us now consider the 2D configuration with an infinite line source:

$$\vec{J}(\vec{r},t) = \hat{y}I_0\delta(x)\delta(z)\,\mathrm{e}^{-i\omega_0 t}\theta(t), \tag{15}$$

where I_0 is just the current flowing in the line source. A straightforward calculation shows that we arrive at Eq. (13) again, but with $\vec{E}^{\,3D}(\vec{r},\omega)$ replaced by:

$$\vec{E}^{\,2D}(\vec{r},\omega) = -\mu_0 I_0\int \vec{\vec{G}}(\vec{r},(0,y',0);\omega)\cdot\hat{y}\,\mathrm{d}y'. \tag{16}$$

For the completeness of our treatment, we also consider the one-dimensional (1D) configuration, in which the source is an infinite current plane:

$$\vec{J}(\vec{r},t) = \hat{y}J_0\delta(z)\,\mathrm{e}^{-i\omega_0 t}\theta(t), \tag{17}$$

where J_0 has the physical meaning of the surface current density of the planar current source. Following the same procedures, we arrive at Eq. (13) with $\vec{E}^{\,3D}(\vec{r},\omega)$ replaced by:

$$\vec{E}^{\,1D}(\vec{r},\omega) = -\mu_0 J_0\int \vec{\vec{G}}(\vec{r},(x',y',0);\omega)\cdot\hat{y}\,\mathrm{d}x'\mathrm{d}y'. \tag{18}$$

Now the remaining problem is to solve Eq. (8) to get $\vec{\vec{G}}(\vec{r},\vec{r}';\omega)$. For this specific geometry, $\vec{\vec{G}}(\vec{r},\vec{r}';\omega)$ has been obtained in Ref. [13]. The essential idea is to expand the solution in each region by a series of plane waves and then determine the expansion coefficients by joining the fields at the boundaries. When $\vec{\vec{G}}(\vec{r},\vec{r}';\omega)$ is known, $\vec{E}^{\,3D}(\vec{r},\omega)$, $\vec{E}^{\,2D}(\vec{r},\omega)$ and $\vec{E}^{\,1D}(\vec{r},\omega)$ can be calculated by Eqs. (14), (16) and (18) straightforwardly. For the focusing problems, usually we are mostly interested in the field distribution in the x–z-plane in the case of $y=0$, and particularly in the imaging region (i.e., $z<-3d/2$). Under these conditions, we obtain:

$$\begin{aligned}E_y^{3D}(x,z;\omega) &= -\frac{i\mu_0 P_0}{8\pi}\int\frac{1}{k_z}\,\mathrm{e}^{-ik_z z}[T^{\mathrm{TE}}(k_{||})(J_0(k_{||}x)-J_2(k_{||}x))\\ &\quad + \frac{k_z^2}{k^2}T^{\mathrm{TM}}(k_{||})(J_0(k_{||}x)+J_2(k_{||}x))]k_{||}\,\mathrm{d}k_{||},\end{aligned} \tag{19}$$

$$E_y^{2D}(x,z;\omega) = -\frac{i\mu_0 I_0}{4\pi}\int\frac{\mathrm{e}^{ik_x x}}{k_z}T^{\mathrm{TE}}(k_x)\,\mathrm{e}^{-ik_z z}\,\mathrm{d}k_x, \tag{20}$$

$$E_y^{1D}(z;\omega) = -\frac{i\mu_0 J_0}{2k}T^{\mathrm{TE}}(0)\,\mathrm{e}^{-ikz}, \tag{21}$$

where $J_n(z)$ are the usual Bessel functions, $k_{||}^2+k_z^2=k^2=(\omega/c)^2$. Here, the transmission coefficients T^{TE} and T^{TM} are given by

$$T^{\mathrm{TE}}(k_{||}) = \frac{4\Delta\,\mathrm{e}^{-ik_z d}}{(\Delta+1)^2\,\mathrm{e}^{-ik_{1z}d}-(\Delta-1)^2\,\mathrm{e}^{ik_{1z}d}}, \tag{22}$$

$$T^{\mathrm{TM}}(k_{||}) = \frac{4\Delta'\,\mathrm{e}^{-ik_z d}}{(\Delta'+1)^2\,\mathrm{e}^{-ik_{1z}d}-(\Delta'-1)^2\,\mathrm{e}^{ik_{1z}d}}, \tag{23}$$

where $\Delta = k_{1z}/k_z\mu_r^L$, $\Delta' = k_{1z}/k_z\varepsilon_r^L$ and $k_{||}^2+k_{1z}^2 = k_1^2 = \varepsilon_r^L\mu_r^L(\omega/c)^2$. The fields in other regions can be obtained similarly.

3. The adaptive-grid technique and a Benchmark result

In this section, we first discuss an important computational technique, and then present a benchmark

result to test the validity of our theory. In all our numerical calculations presented in this paper, we assume that $\varepsilon_r^L(f) = \mu_r^L(f) = 1 - 200/f(f + i\gamma)$ and $d = 10$ mm. We note that

$$\varepsilon_r^L(f) = \mu_r^L(f) \approx -1 + 0.4(f - 10) + i0.2\gamma \qquad (24)$$

in the limit of $f \to 10$, $\gamma \to 0$. This indicates that the lens is a *super* lens with $\delta = 0.4(f-10) + i0.2\gamma$ in this limit, and becomes a *perfect* lens when the condition $f = 10$, $\gamma = 0$ is *exactly* satisfied.

According to the methodology developed in the last section, we can calculate $\vec{E}(\vec{r}, t)$ by two integrations, namely Eqs. (13), (19) and (20). However, in both integrations, we encounter singularities. While the pole of integration in Eq. (13) is obvious, we check Eqs. (19) and (20) to see the origin of the divergences in these integrations. Taking $T^{\mathrm{TE}}(k_{||})$ as an example, according to Eq. (22), we find that it diverges when the condition $(\Delta + 1)^2 e^{-ik_{1z}d} - (\Delta - 1)^2 e^{ik_{1z}d} = 0$ is met. After some simple algebra, we rewrite the condition as:

$$2\cos h(-ik_{1z}d) + (\Delta + \Delta^{-1})\sin h(-ik_{1z}d) = 0. \qquad (25)$$

Eq. (25) is essentially the same as Eq. (3) of Ref. [17], which is the condition to find the transverse-electric (TE)-mode surface wave (SW) excitation of the present geometry (see also Refs. [18,19]). This is physically reasonable, since an SW excitation is an intrinsic EM wave eigen-solution, which exists in the *absence* of an incident evanescent wave. As a result, the response would be *infinite* if the incident wave is *not* zero. Similarly, T^{TM} diverges at the SW excitation of a transverse-magnetic (TM) mode [17–19]. With the presence of finite η and γ, the integrands in Eq. (13) and Eqs. (19) and (20) will be finite but still very large near the poles. Integrations with a conventional method are very difficult to reach convergences. Here, we introduce an adaptive-grid method to deal with these singularities. In our numerical integrations for Eqs. (13), (19) and (20), instead of adopting uniform grids, we take the grid size at a particular ω or k point to satisfy

$$\Delta\omega = \left(\frac{\omega_{\max}}{N_\omega^0}\right)\left[1 + \left|\frac{1}{\omega - \omega_0 + i\eta}\right|\right]^{-1}, \qquad (26)$$

$$\Delta k_{||} = \left(\frac{k_{\max}}{N_k^0}\right)[1 + |T^{\mathrm{TE}}(k_{||})|]^{-1}, \qquad (27)$$

$$\Delta k_{||} = \left(\frac{k_{\max}}{N_k^0}\right)[1 + |T^{\mathrm{TM}}(k_{||})|]^{-1}, \qquad (28)$$

where $\omega_{\max}$ and $k_{\max}$ are the cut-off values of ω and k taken in the numerical integrations, and N_ω^0 and N_k^0 and some integers. Eq. (26) shows clearly that the grid size, $\Delta\omega$, approaches $(\omega_{\max}/N_\omega^0)$ when far away from the singularity ω_0, but becomes significantly reduced in the vicinity of the pole. The same is true for the k grid seen from Eqs. (27) and (28). By doing so, we *automatically* sample more points around the singularities where we really care, and less points when far away from the singularities where the contribution to the integral is small.

We now check the calculation convergences by computing the value of $E_y^{2D}(\vec{r}, \omega)$ at $\vec{r} = (0, 0, -3d/2)$ and $\omega = 2\pi \times 9.98$ GHz with $\gamma = 10^{-5}$ GHz as an example. We first consider the integration convergence against $k_{\max}$. In the integrations with different $k_{\max}$ values, we adjust N_k^0 to ensure that $(k_{\max}/N_k^0) = ((\omega/c)/500)$ is the same in each case. The solid symbols depicted in Fig. 1(a) show that the calculation converges quickly when $k_{\max} \gg k_{\mathrm{pole}} \sim 2.8(\omega/c)$. This is reasonable, since $T^{\mathrm{TE}}(K_{||}) \to 0$ as long as $k_{||} \gg k_{\mathrm{pole}}$ with k_{pole} being the SW pole value for this frequency. We then consider the integration convergence against the number of k points taken. Shown in Fig. 1(b) are the results calculated with different k points but with the same cut-off value, $k_{\max} = 10\,\omega/c$, which shows again

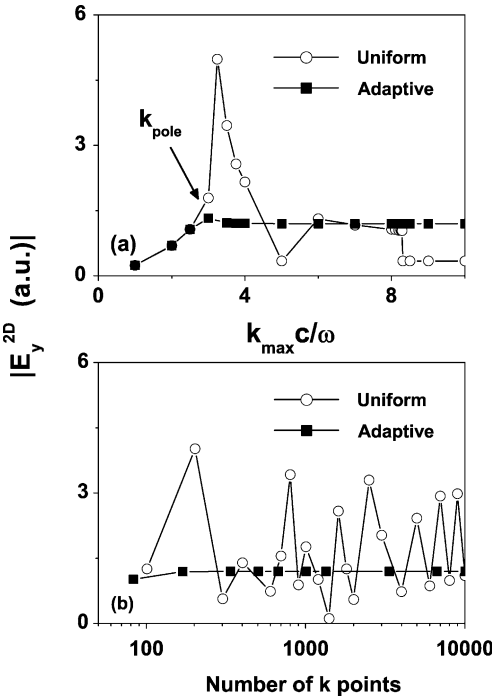

Fig. 1. Convergences of the integrations against (a) $k_{\max}$ and (b) the number of k points in the uniform-grid method and the adaptive-grid method.

that the calculation converges very quickly. We now employ a uniform-grid to do the *same* calculations and compare the results with those of the adaptive-grid method in Fig. 1(a) and (b). We note from Fig. 1(a) that the uniform-grid method goes to a *wrong* result, although it does seem to converge when $k_{\max}$ is big enough. From Fig. 1(b), we find that the uniform-grid result fluctuates dramatically against varying the number of k points, and the calculation does not seem to converge with even 10 000k points. In contrast, the adaptive-grid method only requires about 200k points to reach convergence, much more efficient than the uniform-grid method. The physics is quite simple. In the uniform-grid method, most of k points are wasted in sampling the regions far away from the singularity, but in regions near the poles, the grid size is still not small enough to ensure convergence.

We now present a benchmark result to demonstrate the validity of our approach. Without scatterings (i.e., set $\varepsilon_r^L = \mu_r^L = 1$), the 1D model can be exactly solved. In this case, we have $T^{\mathrm{TE}} = 1$ so that Eq. (21) becomes

$$E_y^{1D}(z;\omega) = -\frac{i\mu_0 J_0 c}{2\omega}\,\mathrm{e}^{-i(\omega/c)z}. \tag{29}$$

Inserting the above equation into Eq. (13), we obtain:

$$\begin{aligned} E_y^{1D}(z,t) &= -\frac{i\mu_0 J_0 c}{4\pi}\int \mathrm{d}\omega\,\frac{\mathrm{e}^{-i\omega(t+z/c)}}{\omega-\omega_0+i\eta} \\ &= -\frac{i\mu_0 J_0 c}{4\pi}\theta\left(t+\frac{z}{c}\right)(-2\pi i)\,\mathrm{e}^{-i\omega_0(t+z/c)} \\ &= -\frac{\mu_0 J_0 c}{2}\,\mathrm{e}^{-i\omega_0(t+z/c)}\theta(t+z/c), \end{aligned} \tag{30}$$

which is a completely causal result (note $z < 0$ here). It is emphasized that the positive sign of η is necessary to obtain this causal result. We then compare the direct numerical integration based on our theory with the analytical expression (30). Shown in Fig. 2 are the calculated $E_y^{1D}(z,t)$ as the functions of time using our theory. In the calculations, we set $\omega_{\max} = 2\pi \times 80$ GHz, $\omega_0 = 2\pi \times 10$ GHz, $\eta = 10^{-4}$ GHz, $z = -20$ mm, and $N_\omega^0 = 7000$. We note that the direct calculation results are in good agreement with the analytical expression (30), although there exists some typical fluctuations caused by adopting a finite cut-off frequency.

4. Applications of the theory

We present some examples to illustrate the applications of our theory. The first example is a 3D focusing problem, with parameters set as $\omega_0 = 2\pi \times 10$ GHz,

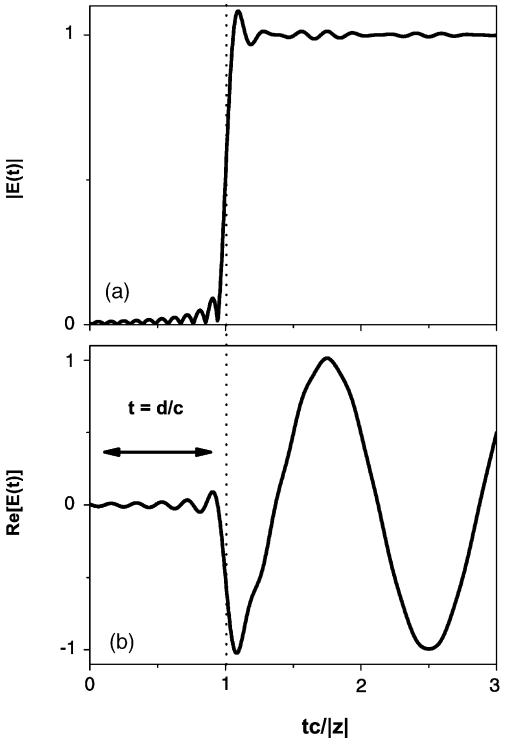

Fig. 2. The amplitude (a) and the real part (b) of $E_y^{1D}(z,t)$ (in units of $\mu_0 J_0 c/2$) as the functions of time.

$\gamma = 0.001$ GHz, $\eta = 0.0005$ GHz. On the image plane at $z = -20$ mm, we calculated the field distribution along x direction for $y = 0$ (i.e., $|E_y^{2D}|$ as a function of x) at different time instances. The patterns are shown together in Fig. 3. It clear that as t increases, the image point becomes brighter and brighter, and the other regions become darker and darker. If we define a quantity w as the peak width measured at its half-maximum, we see clearly that w is a decreasing function of time, indicating that the resolution becomes better and better as t increases. As a reference, we set $k_{\max} = \omega/c$ in our numerical integration of Eq. (19) to do a calculation *without* evanescent waves, and depict the calculated pattern in Fig. 3(b). Compared with Fig. 3(a), we find that the peak of the reference pattern is much broader and the field is much weaker. This suggests clearly that the resolution enhancement is contributed by the evanescent waves only, and also the super-imaging is established through the dynamics of the evanescent waves.

We now consider a 2D focusing problem as another example. It has been understood that a non-zero δ is crucial in such problems. In the 2D geometry, all previous time-domain studies considered the situation of δ being purely imaginary [6–11]. Although it was

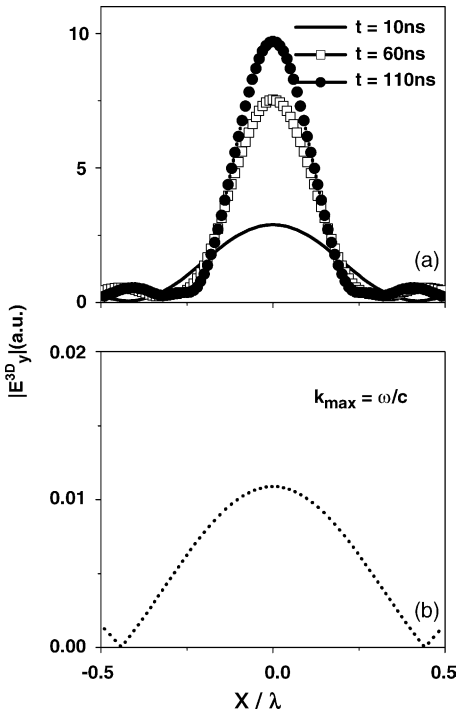

Fig. 3. (a) Field patterns at different time instances. (b) Field pattern calculated by considering only the propagating components of the source.

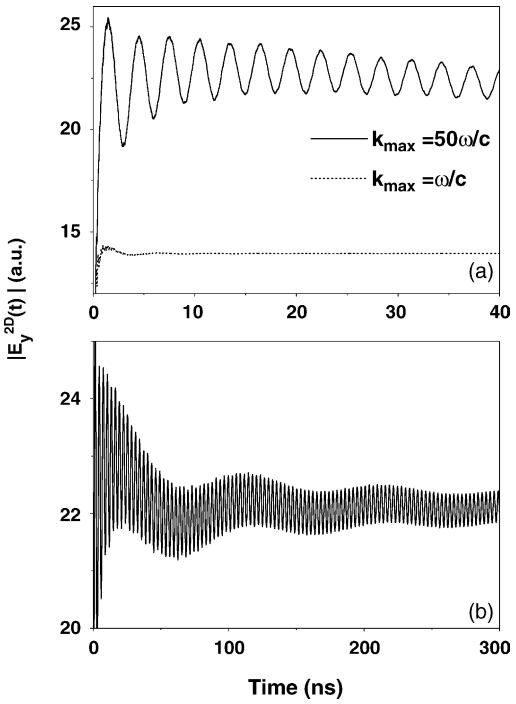

Fig. 4. (a) Time evolution of $|E_y^{2D}|$ at the image point in a 2D focusing process (with $f_0 = 9.99$ GHz, $\gamma = 0.0005$ GHz, $\eta = 0.001$ GHz) calculated by considering all components (solid) and propagating waves only (dashed). (b) Same as (a) but with a larger observing time scale.

suggested that a real δ is also helpful to avoid the field divergence in the 2D metamaterial lens focusing [5], very few time-domain studies were performed on such lensing problems. Here, we show a typical example to illustrate the time-domain relaxations in 2D focusing with δ being generally complex. We choose $f_0 = 9.99$ GHz, $\gamma = 0.0005$ GHz such that $\delta = -0.004 + 10^{-4}i$ at the working frequency, according to Eq. (24). For this system, we employed our theory to calculate the time evolution of the field amplitude at the image point, and show the result in Fig. 4(a) as a solid line. We find the time evolution to be accompanied by strong field oscillations, and such oscillations are apparently contributed by the evanescent waves, since the calculation with only propagating waves included (dashed line) does not show any oscillation. Compared with the case of δ being purely imaginary [7,15], the presence of a nonzero Re(δ) does not seem to produce any new phenomenon in the time evolution. For example, compared with Fig. 1 of Ref. [15], even the oscillation period is almost the same, indicating that the present oscillation must be governed by the same physics [15]. However, when we expand the observing time scale to a larger value as shown in Fig. 4(b), we find very clearly a long-period oscillation over the short-period oscillation. This phenomenon was not found in previous studies for the 2D focusing with a purely imaginaryδ [7,15]. This long-period oscillation is mainly caused by Re(δ) and disappears when Re(δ) = 0, and it shares the similar physical origin with that discussed in Ref. [16] for the 3D focusing problem.

5. Conclusions

To conclude, we present in this paper a time-dependent Green's function approach to study the transient behaviors of optical processes related to metamaterials, in particular, the super lens focusing. The approach can be easily extended to study other optical processes, if $\overrightarrow{\overrightarrow{G}}(\vec{r}, \vec{r}'; \omega)$ are calculated for that particular problem. We have introduced an adaptive-grid method to deal with the singularities encountered in the numerical integrations, which greatly enhances the calculation efficiency and makes the computations tractable. A benchmark result is presented to demonstrate the validity of our theory. To illustrate the applications of present theory, we have implemented the method to study two typical focusing processes with metamaterial lenses.

Acknowledgements

This work was supported by National Basic Research Program of China (No. 2004CB719800), Program for Changjiang Scholars and Innovative Research Team in University, Shanghai Science and Technology Committee, National Natural Science Foundation of China (No. 10504003) and Hong Kong RGC through CA02/03.SC01.

References

[1] V.C. Veselago, Sov. Phys. Usp. 10 (1968) 509.
[2] J.B. Pendry, Phys. Rev. Lett. 85 (2000) 3966.
[3] N. Garcia, M. Nieto-Vesperinas, Phys. Rev. Lett. 88 (2002) 207403.
[4] J.B. Pendry, Phys. Rev. Lett. 91 (2003) 099701.
[5] D.R. Smith, D. Schurig, M. Rosenbluth, S. Schultz, S.A. Ramakrishna, J.B. Pendry, Appl. Phys. Lett. 82 (2003) 1506.
[6] R.W. Ziolkowski, E. Heyman, Phys. Rev. E 64 (2001) 056625.
[7] X.S. Rao, C.K. Ong, Phys. Rev. B 68 (2003) 113103.
[8] X.S. Rao, C.K. Ong, Phys. Rev. E 68 (2003) 067601.
[9] S.A. Cummer, Appl. Phys. Lett. 82 (2003) 1503.
[10] P.F. Loschialpo, D.L. Smith, D.W. Forester, F.J. Rachford, J. Schelleng, Phys. Rev. E 67 (2003) 025602(R).
[11] L. Chen, S.L. He, L.F. Shen, Phys. Rev. Lett. 92 (2004) 107404.
[12] R. Merlin, Appl. Phys. Lett. 84 (2004) 1290.
[13] Y. Zhang, T.M. Grzegorczyk, J.A. Kong, Electromag. Waves 35 (2002) 271.
[14] G. Gomez-Santos, Phys. Rev. Lett. 90 (2003) 077401.
[15] L. Zhou, C.T. Chan, Appl. Phys. Lett. 86 (2005) 101104.
[16] L. Zhou, C.T. Chan, Opt. Lett. 30 (2005) 1812.
[17] L. Zhou, C.T. Chan, Appl. Phys. Lett. 84 (2004) 1444.
[18] R. Ruppin, J. Phys.: Condens. Matter 13 (2001) 1811.
[19] B.I. Wu, T.M. Grzegorczyk, Y. Zhang, J.A. Kong, J. Appl. Phys. 93 (2003) 9386.